

# THEORETICAL AND EXPERIMENTAL RESEARCH OF ULTRA-HIGH-PERFORMANCE CONCRETE TENSILE BEHAVIOUR BASED ON MICRO-ANALYSIS

LIU XINYI\*, ZHANG RONGLING, DUAN YUN

*National and Provincial Joint Engineering Laboratory of Road & Bridge  
Disaster Prevention and Control, Lanzhou Jiaotong University,  
Lanzhou 730070, PR China*

Received 11 July 2022; accepted 11 January 2023

**Abstract.** The cracking resistance and durability of the ultra-high-performance concrete (UHPC) structure are directly affected by its tensile behaviour. A micro-analysis method was established to study the tensile behaviour of the UHPC before the appearance of visible cracks. The cooperative characteristic of the steel fibre and the cement matrix was taken as a research focus of the micro-analysis method. The random distribution of steel fibre was considered as normal distribution. Based on the micro-analysis method, the tensile behaviour of UHPC was divided into the elastic stage and micro-damage development stage. Other data sourced elsewhere were used to verify the feasibility of the micro-analysis method and the necessary data were tested using pure bending specimens to verify the theoretical model. The results show that the working mechanism of inner steel fibre can be described by the micro-analysis method. The bending test results of the UHPC at the elastic and the micro-damage development stage match the theoretical model. The tensile behaviour of the UHPC is dominated by the inner steel fibre and the contribution of the cement matrix can be ignored. A bilinear model is proposed to describe the tensile constitutive of UHPC before the appearance of visible cracks, and the limitations of each stage are 8.85 MPa and 12.36 MPa.

\* Corresponding author. E-mail: [lxy-ql@mail.lzjtu.cn](mailto:lxy-ql@mail.lzjtu.cn)

Liu XINYI (ORCID ID 0000-0003-3431-9178)

Copyright © 2023 The Author(s). Published by RTU Press

This is an Open Access article distributed under the terms of the Creative Commons Attribution License (<http://creativecommons.org/licenses/by/4.0/>), which permits unrestricted use, distribution, and reproduction in any medium, provided the original author and source are credited.

**Keywords:** bilinear model, micro-analysis method, non-uniform distribution, steel fibre, steel fibre reinforced UHPC, ultra-high-performance concrete.

## Introduction

With the rapid development of engineering construction, new types of cement matrix materials have been developed. Among them, ultra-high-performance concrete (UHPC) (Russell & Graybeal, 2013), which earns better performance (AFGC/SETRA, 2013; Russell & Graybeal, 2013), has been proved to be a promising candidate (Park et al., 2012; Aaleti et al., 2013; Randl et al., 2014; Graybeal, 2006; Wille & Naaman, 2012) because of its unique performance (Noori et al., 2015; Johnston, 2011). The tensile ductility and toughness (Lee & Barr, 2004) of UHPC are important properties, which ensure structural safety. The matrix of UHPC is extremely dense and the steel fibres are randomly mixed to improve the strength and ductility performance. Because of its advanced mix design method, the tensile behaviour of UHPC is much better than ordinary concrete. Due to its metal-like tensile properties, tensile UHPC is completely different from ordinary concrete.

Accurate determination of the tensile stress-strain relation is a prerequisite to analyse the tensile behaviour of UHPC structures. Extensive research has been conducted into the tensile constitutive model of UHPC. The inner steel fibre is an important determinant, and the bonding action between the steel fibre and cement matrix has been studied in many experiments. Orange et al. (1999) studied the bonding behaviour of single flat steel fibre with different embedded depth, fibre diameter and surface roughness. Chan & Chu (2004) concluded that the optimal content of the silicon powder should be 20%–30% to obtain a good bonding action. Wille & Naaman (2010) fitted the stress-slip formula of the bonding action between the steel fibre and the cement matrix using nine groups of flat steel fibre with different sizes and three groups of steel fibre with different shapes. The influence of the steel fibre on the tensile working behaviour of UHPC was investigated on the basis of the bonding action between the steel fibre and the cement matrix. Park et al. (2012) and Wille & Naaman (2012) demonstrated the effect of fibre shape and geometry on the tensile behaviour of UHPC. Kang & Kim (2011) studied the response of fibre orientation distribution after cracking under tensile condition. To obtain the necessary ductility and toughness, Zhang (2016) summarised other published results and indicated that the UHPC should be mixed with more than 2% straight steel fibre with the diameters of 0.15–0.4 mm and lengths of 6–15 mm.

To explore the stress-distribution mechanism of the UHPC, several flexural design methods were developed. Barros et al. (2005) suggested that the tensile constitutive model of RILEM TC 162-TDF (Rilem, 2003) was suitable for design calculation relating to UHPFRC structures. Meanwhile, several tensile constitutive models were proposed such as the ascending-horizontal model (Ai-Osta et al., 2017), the ascending-descending model (Van & Mbewe, 2013) and the multi-segment linear model (Habel et al., 2004). The feasibility of these models was limited due to their large number of undetermined coefficients. Few micro-mechanical behaviour models were established for tensile UHPC, such as the relationship between micro bonding action of the steel fibre and the bearing capacity. Lok & Pei (1998) established a strain-hardening tensile constitutive model, which included the influence of fibre volume content and fineness ratio. Singh (2015) established a flexural strength model based on strain compatibility and force equilibrium, which took the distribution and orientation of steel fibre into consideration. Qi et al. (2018) proposed a mesoscale mechanical model for ultra-high-performance fibre reinforced concrete, which could reflect the effect of fibre distribution, embedment length and fibre orientation.

The aforementioned models are semi-empirical and not sufficient to describe the tensile behaviour of the steel fibre theoretically as well as the bonding action between steel fibre and cement matrix (Ghafari et al., 2014; Kang et al., 2017). Those methods cannot describe the essence of the force in the fibre because the fibre force is simply assumed to be an active force for discussion. Although some relational models (Qi et al., 2018; Huang, 2004) between the cement matrix strain and the fibre force are proposed by assuming an embedment length for steel fibre, the whole calculation still relies on the assumed active fibre force. When the tensile UHPC component balances the external load, the inner steel fibres are loaded by the cement matrix, which means that the fibre force is reactive force. Therefore, when establishing the tensile behaviour model of UHPC, the difficulty is to reveal the true stress pattern of steel fibre and the logical bonding relationship between the cement matrix and the steel fibre. Thus, the key to analysis of the tensile behaviour of UHPC is to determine the loading pattern of the cement matrix on the steel fibre.

By clarifying the steel fibre force as reactive force, a micro-analysis method of steel fibre was established based on a cooperative behaviour between the cement matrix and the steel fibre. The stress distribution in the steel fibre is non-uniform in this method. The tensile working mode of the steel fibre is divided into two stages by the formation of the micro-damage to the cement matrix, defined as elastic stage and micro-damage development stage. Based on the description of the working condition of the steel fibre before cracking, a tensile constitutive model of UHPC

under pure bending load is proposed. The micro-analysis method was verified by four-point bending test as well as published data.

## 1. Micro-analysis of steel fibre

### 1.1. Model assumptions

Steel fibre reinforced UHPC is studied. Several basic assumptions can be used in order to simplify the analysis: (1) UHPC follows the basic assumptions of material mechanics before cracking; (2) the fibres are short and straight; (3) the Poisson effect of the steel fibre is neglected; (4) the cement matrix and the steel fibre are isotropic; (5) any two of the fibres are relatively independent.

For readability purposes, the main letters are used to denote the following:

- $F_U$  the total axial force on the UHPC composite section;  
 $F_f$  the resultant force on the steel fibres;  
 $F_c$  the axial force on the cement matrix;  
 $\sigma_U$  the tensile stress on UHPC;  
 $\sigma_f$  the component stress on the steel fibre;  
 $\sigma_c$  the tensile stress on the cement matrix;  
 $n$  the number of the steel fibre at the cross-section of interest;  
 $\rho_f$  the volume fraction of the steel fibre;  
 $\rho_c$  the volume fraction of the cement matrix;  
 $\varepsilon_U$  the strain of UHPC;  
 $\tau_f(\theta, z)$  the bonding action on the steel fibre loaded by surrounding cement matrix;  
 $P_f$  the external force on the steel fibre;  
 $\sigma(z)$  axial stress on the steel fibre at any section in terms of  $z$ .

### 1.2. Tensile working pattern of UHPC

The internal force on tensile UHPC at any cross-section can be expressed as:

$$F_U = F_f + F_c, \quad (1)$$

$$F_U = \sigma_U A_U, \quad (2)$$

$$F_f = n \cdot \sigma_f \cdot A_f, \quad (3)$$

$$F_c = \sigma_c A_c, \quad (4)$$

where  $F_U$  represents the total axial force on the UHPC composite section,  $F_f$  represents the resultant force on the steel fibres and  $F_c$  represents the

axial force on the cement matrix. The  $\sigma_U$  is the tensile stress on UHPC,  $\sigma_f$  is the component stress on the steel fibre in the tensile direction and  $\sigma_c$  is the tensile stress on the cement matrix.  $A_U$ ,  $A_f$  and  $A_c$  are the areas of the UHPC at the cross-section, the cross-sectional area of the steel fibre and the sectional area of the cement matrix.  $n$  is the number of the steel fibre at the cross-section of interest.

Substituting Equations (2)–(4) into Equation (1), the stress of UHPC can be simplified as:

$$\sigma_U = \sigma_f \frac{nA_f}{A_U} + \sigma_c \frac{A_c}{A_U} = \sigma_f \rho_f + \sigma_c \rho_c \quad (5)$$

where  $\rho_f$  is the volume fraction of the steel fibre and  $\rho_c$  is the volume fraction of the cement matrix.

The deformation coordination between the steel fibre and the cement matrix is satisfied before the appearance of cement matrix micro-damage. The strain  $\varepsilon_U$  in the UHPC can be described as:

$$\varepsilon_U = \frac{\sigma_f}{E_f} = \frac{\sigma_c}{E_c}, \quad (6)$$

where  $E_f$  and  $E_c$  are the elastic modulus of the steel fibre and the cement matrix, respectively. After the increase of  $\varepsilon_U$ , the increment of  $\sigma_f$  will be much larger than  $\sigma_c$  because  $E_f \gg E_c$ . This relationship reveals that the fibre stress is far more important than cement matrix stress. The contribution of the cement matrix force can be ignored. Based on this method, the subsequent calculations can be simplified without excessive error and compromise with regard to factor of safety.

Thus, the key to this theoretical analysis is to describe the working condition of the steel fibre. The tensile condition of steel fibre is analysed from two perspectives, which are random orientation and bonding action loaded by cement matrix.

### 1.2.1. Random orientation of steel fibre

For steel fibre reinforced concrete, the steel fibres are randomly distributed in the concrete. The reinforcing efficiency is optimal when the steel fibre is parallel to the stress direction and the efficiency is the worst when the steel fibre is perpendicular to the applied stress. An effective coefficient of fibre orientation (Huang, 2004) is proposed to describe the relationship between the random fibre orientations and the enhancement efficiency. Thereof, this is given in terms of the specific value of net force between random fibre and oriented fibre along with the loading orientation.

A coordinate system was established (Figure 1) with the  $x$ -axis parallel to the applied tensile force. The fibre length is  $l$  and fibre distributions can be described by one-dimensional stochastic variable  $\alpha$ . A conical surface is formed by all possible distribution with the same enhancement coefficient. The angle  $\alpha$  can be treated as a continuous random variable expected value  $\mu$ ; thus, the enhancement coefficient for  $x$  can be simply described as  $\cos \mu$ .

### 1.2.2. Bonding action of steel fibre

A cylindrical coordinate system ( $\rho, \theta, z$ ) is established (Figure 2a). The bonding action  $\tau_f(\theta, z)$  on the steel fibre loaded by surrounding cement matrix is a function in terms of variable  $\theta$  and  $z$ . The steel fibre is always in tension so the bonding action forms a couple. Since the fibre radius  $r$  is much smaller than the fibre length  $l$ ,  $\tau_f(\theta, z)$  can be assumed to be uniformly distributed around the circumference. Thus, the bonding action at any cross-section  $dz$  can be described as  $2\pi r\tau_f(z) dz$  in terms of  $z$ . The bonding action is related to the strain component of cement matrix parallel to the fibre direction. The bonding action can be described using Equation (7) before reaching its limits.

$$\tau_f(z) = D_f \cdot \varepsilon_c \cdot \cos \mu, \quad (7)$$

where  $D_f$  is the relationship between the tensile strain  $\varepsilon_c \cdot \cos \alpha$  of cement matrix and bonding condition  $\tau_f(z)$ . The unit of  $D_f$  is  $\text{N}/\text{mm}^2$  that can be obtained experimentally. The loaded steel fibre is in equilibrium and the external force on the steel fibre  $P_f$  is:

$$P_f = 2\pi r \int_0^l \tau_f(z) dz = 0. \quad (8)$$

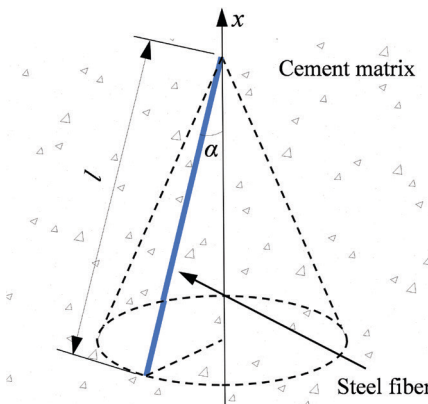


Figure 1. Distribution model of steel fibre

$l_1$  and  $l_2$  are any two points on the steel fibre shown in Figure 2b. The equilibrium condition can always be described as:

$$\sigma(l_1)A_f + 2\pi r \int_{l_1}^{l_1+l_2} \tau_f(z)dz = \sigma(l_1+l_2)A_f, \quad (9)$$

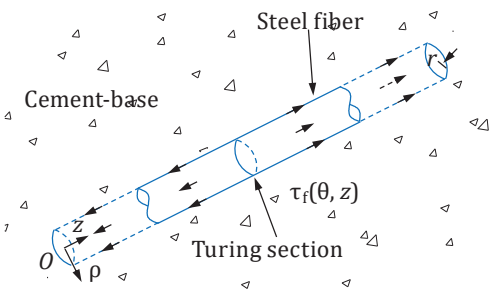
where  $\sigma(z)$  is the axial stress on the steel fibre at any section in terms of  $z$ , while  $\sigma(l_1)$  and  $\sigma(l_1+l_2)$  are the axial stress on section  $z=l_1$  and  $z=l_1+l_2$ .

The axial stress on the steel fibre at any section can be described as:

$$\sigma(z) = \frac{2\pi r}{A_f} \int_0^z \tau_f(z)dz. \quad (10)$$

The stress distribution of steel fibre is non-linear along the fibre axis based on Equation (10), which is inconvenient for further calculation as shown in Figure 3a. The calculation of strain can be simplified by referring to the mean equivalent value shown in Figure 3b. The mean stress  $\sigma_f$  is given by the equality as shown in Equation (11) at  $l_a$  and

a) Stress condition of the steel fibre



b) Stress analysis of the steel fibre

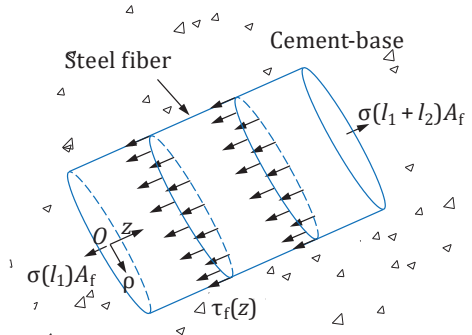
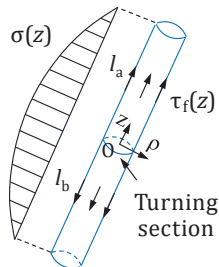


Figure 2. Micromechanical tensile behaviour model of steel fibre

a) Axial stress distribution



b) Mean stress distribution

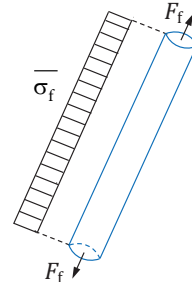


Figure 3. Sketches of the stress distribution

$l_b$  because the bonding force between these two parts is equivalent inverted.

$$\bar{\sigma}_f = \frac{1}{l_a} \int_0^{l_a} \sigma(z) dz = \frac{2\pi r}{A_f l_a} \int_0^{l_a} \tau_f(z) dz dz = \frac{1}{l_b} \int_0^{l_b} \sigma(z) dz = \frac{2\pi r}{A_f l_b} \int_0^{l_b} \tau_f(z) dz dz. \quad (11)$$

Substituting Equation (7) into Equation (11), the tensile stress of steel fibre in Equation (3) can be described as:

$$\bar{\sigma}_f = \sigma_f \cdot \cos \mu = \frac{2D_f \pi r \cos^2 \mu}{A_f l_a} \int_0^{l_a} \varepsilon_c dz dz = \frac{2\pi r D_f \cos^2 \mu}{A_f l_b} \int_0^{l_b} \varepsilon_c dz dz. \quad (12)$$

## 2. Tensile behaviour of UHPC

From the above results, the tensile behaviour of UHPC is dominated by the inner steel fibre. The contribution of the cement matrix to the axial force of tensile UHPC can be ignored; thus, the  $\sigma_U$  can be rewritten by considering the enhancement efficiency along the  $x$ -axis and ignoring the contribution of the cement matrix.

$$\sigma_U = \frac{2\pi r D_f \rho_f \cos^2 \mu}{A_f l_a} \int_0^{l_a} \varepsilon_c dz dz = \frac{2\pi r D_f \rho_f \cos^2 \mu}{A_f l_b} \int_0^{l_b} \varepsilon_c dz dz. \quad (13)$$

As a cement matrix material, UHPC should show the same cracking pattern with ordinary concrete. The visible cracks are formed through the formation and expansion of micro-scale damage (Guo, 1997). UHPC can be assumed to have no initial defects because of the maximum density design theory. Only the undamaged cement matrix can provide a continuous bonding force and the bonding action  $\tau_f(z)$  will change with the appearance of the micro-damage. Thus, the fibre stress pattern can be divided into two stages. One stage is before the formation of micro-damage, and the other is after the appearance of micro-damage.

### 2.1. Stress distribution at the first stage

The cement matrix is undamaged in the first stage (elastic stage). The strain distribution is uniformly continuous under uniaxial tensile condition (Figure 4).

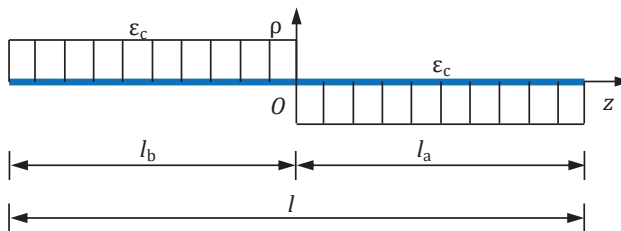


Figure 4. Stress distribution pattern of steel fibre under tensile load

The  $\varepsilon_c$  is not a function in terms of  $z$  so the stress on the UHPC under tensile condition can be deduced by using Equation (13):

$$\sigma_U = \frac{\pi r D_f \varepsilon_c \rho_f l \cos^2 \mu}{2 A_f} \quad (14)$$

The strain distribution is different under bending and changes linearly with distance from the neutral axis. The turning section plane of fibres move to one end as shown in Figure 5.

The heights  $h_a$ ,  $h_b$  are the length between the two ends of the steel fibre and the neutral axis.  $h_0$  is the length between the turning section and the neutral axis. Thus, the cement matrix strain  $\varepsilon_c$  around the steel fibre can be described in terms of the strain  $\varepsilon_c^0$ :

$$\frac{\varepsilon_c^0}{\varepsilon_c} = \frac{h_0}{h_0 - \frac{h_b - h_a}{l} z} \quad (15)$$

$$\varepsilon_c = \left( 1 - \frac{h_b - h_a}{h_0 l} z \right) \varepsilon_c^0 = (1 - kz) \varepsilon_c^0 \quad (16)$$

where the parameter  $k$  is the strain slope in the local coordinate system. The bonding action  $\tau_f(z)$  under bending is:

$$\tau_f(z) = D_f \varepsilon_c = D_f (1 - kz) \varepsilon_c^0 \quad (17)$$

Substituting Equation (17) into Equation (14):

$$\sigma_t = \frac{\pi r D_f \rho_f \varepsilon_c^0 \cos^2 \mu}{A_f} \left( l_a - \frac{k l_a^2}{3} \right) = \frac{\pi r D_f \rho_f \varepsilon_c^0 \cos^2 \mu}{A_f} \left( l_b + \frac{k l_b^2}{3} \right) \quad (18)$$

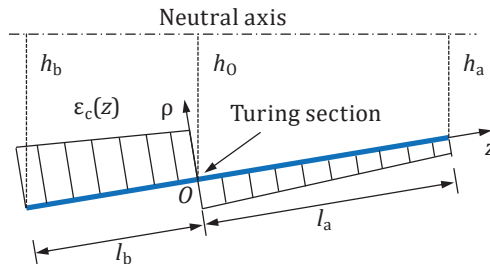


**Figure 5.** Stress distribution pattern of steel fibre under bending condition

## 2.2. Stress distribution in the second stage

After the bonding strength reaches its limit, micro-damage will form and develop in the second stage. Visible cracks cannot be observed at this stage, so the second stage is called the micro-damage development stage. There are two situations seen in the micro-damage development stage: (1) only one feature related to damage is formed (Figure 6a); (2) several damages extend (Figure 6b).

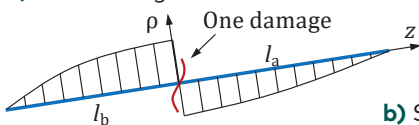
The bonding condition can be transformed from that shown in Figure 6(a) to that in Figure 6(b) and this process is unpredictable. The distribution of bonding action at  $l_a$  and  $l_b$  is different, but the equilibrium condition is always satisfied, because the resultant bonding force at two ends of the steel fibre is equal and opposite, the bonding action at the middle part can be ignored. By comparing the results of tests on rebar (Liang & Shi, 2011), the bonding action at  $l_a$  and  $l_b$  is non-linear so the parameters are too numerous to be determined by equilibrium and boundary conditions. The tensile condition of the steel fibre at micro-damage development stage is given based on Equation (13):

$$\sigma_U = \frac{2\pi r D_f \rho_f \cos^2 \mu}{A_f l_a} \int_0^{l_a} \int_0^z \varepsilon_a(z) dz dz = \frac{2\pi r D_f \rho_f \cos^2 \mu}{A_f l_b} \int_0^{l_b} \int_0^z \varepsilon_b(z) dz dz, \quad (19)$$

where  $\varepsilon_a(z)$  and  $\varepsilon_b(z)$  are unknown function in terms of bonding action at  $l_a$  and  $l_b$ . The stress-strain curve at the micro-damage development stage is random.

The main difference between the elastic stage and the micro-damage development stage is the stress distribution and the effective working length of the steel fibres. The effective working length at the elastic stage is the fibre length  $l$  and the working length at the micro-damage

### a) One damage



### b) Several damages

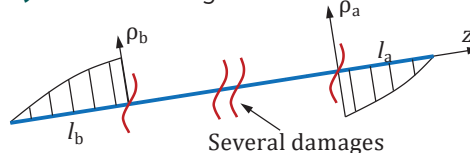


**Figure 6.** Stress distribution pattern of steel fibre at micro-damage development stage

development stage is less than  $l$ . The shift from the elastic stage to the micro-damage development stage significantly reduces the working length of steel fibres. This decrease of the working length can cause a significant reduction in the fibre reinforcing effect. Although the bonding pattern at the micro-damage development stage is unknown and rarely measured, it can still be predicted that the equivalent elastic moduli at the micro-damage development stage is much lower than in the elastic stage.

### 3. Verification of the micro-analysis method

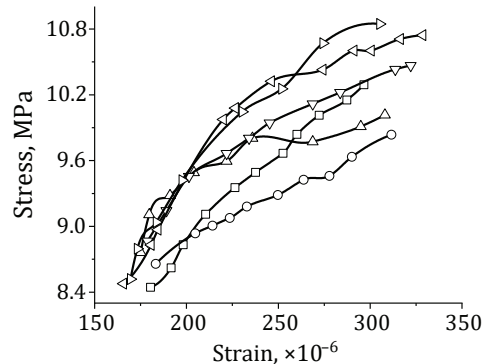
#### 3.1. Feasibility analysis of the micro-analysis method

The micro-analysis method output suggests a constitutive model, including two stress stages for tension UHPC. The non-uniform distribution, orientation of steel fibre and size of steel fibre are taken

Table 1. Tests and theoretical value of elastic limit

Data group	Fibre size, $l/r_{fi}$ mm	Fibre content, %	Tests stress, MPa	Theoretical value, MPa	Percentage of difference
Reference (Zhang, 2016)	8/0.06	2.0	8.28	7.59	8.33%
		2.5	9.62	9.48	1.45%
Reference (Shao et al., 2020)	13/0.11	2.0	9.00	8.98	2.22%
		2.5	9.20	9.18	2.17%
Reference (Shen, 2017)	13/0.10	2.0	8.82	7.64	13.38%
		2.5	9.33	10.02	7.45%

a) Reference (Shao et al., 2020) data



b) Reference (Shen, 2017) data

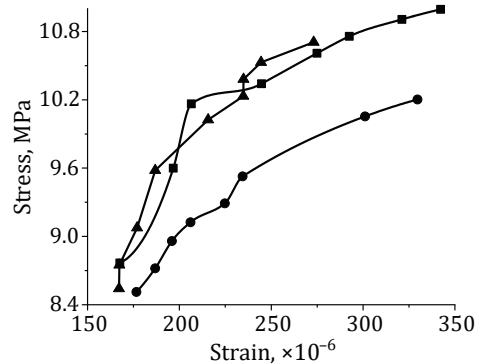


Figure 7. Reference data

into account. In theory, the micro-analysis may be used for different types of steel fibre reinforced concrete.

Different from ordinary concrete with uniform codes/standards, there are many types of UHPC with different formulations in use around the world. The tensile behaviours of these UHPC are significantly different. The feasibility of the micro-analysis method can be verified by reference to the literature. Relying on the micro-analysis method, elastic limit of UHPC with different fibre parameters can be calculated from known data. Reference (Zhang, 2016; Shao et al., 2020; Shen, 2017) data are used to verify the feasibility of the micro-analysis method. The calculated results are shown in Table 1 and match the test results.

The micro-damage development stage is difficult to be identified with precision because the strain measurement and collection methods are all different. Theoretical analysis shows that the micro-damage development stage has the following characteristics: (1) the stress-strain curve is irregular, (2) the limiting values are dispersed. Reference (Shao et al., 2020) data are shown in Figure 7a and reference (Shen, 2017) data are shown in Figure 7b. With the predicted stress-strain relation, both sets of reference data are irregular and difficult to generalise under a similar function. Instead of a similar limiting value at the elastic stage, both strain and stress limits differ.

Although the tensile stress-strain relationship of UHPCs with different formulations varies (Dogu & Menkulasi, 2020), many similar key points are defined such as the elastic limit, cracking point and ultimate limit state. Non-linear constitutive relation inevitably leads to stress redistribution of the specimens. Normal analysis method usually defines the key points by macroscopic test phenomenon, which makes it inconvenient to divide the cracking phase through micro-mechanism type. To verify the stages divided by the micro-analysis method, the data acquisition should be more precise. Thus, the four-point bending test was designed to have a high data-collection frequency.

## **3.2. Bending tests**

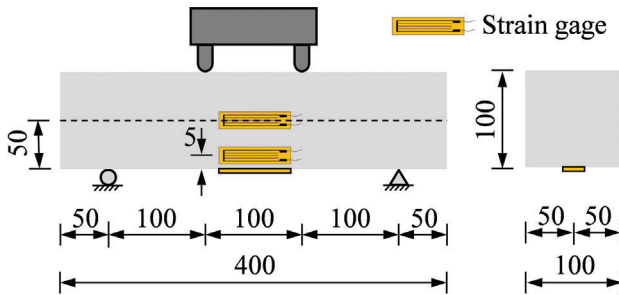
### **3.2.1. Specimen design**

Instead of dividing the stress stages by test data, the micro-analysis method defines two stress stages before the appearance of visible cracking based on different bonding patterns of steel fibre. To verify the micro-analysis method, four-point bending test was designed to obtain necessary data. The used UHPC was mixed with short, straight brass-coated steel fibres and the volume fraction was 2.5%. The length of steel

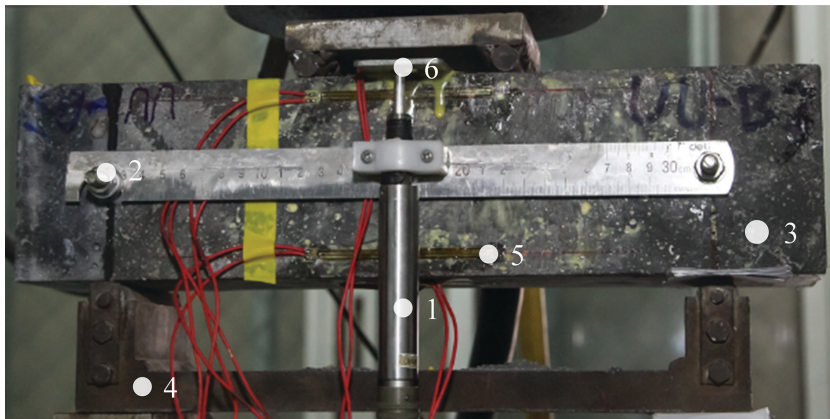
fibre is 12 mm and their diameter is 0.2 mm. The main ingredients of the UHPC are listed in Table 2.

The pure bending length of the beam specimen (100 mm × 100 mm × 400 mm) is 100 mm as shown in Figure 8a. A LVDT (linear variable displacement transducers) was used to measure the mid-span displacement. To eliminate the interference of support and mechanical deformation, the LVDT stands were pivoted at the intersection between the neutral axis of beam and the support extension line (Figure 8b). Although the load-midspan displacement curve is one of the important mechanical properties of tensile UHPC, it cannot directly represent the stress-strain relationship predicted by theoretical derivation. To obtain

a) Specimen for bending test, mm



b) Arrangement of LVDT



- 1 - LVDT
- 2 - LVDT stands
- 3 - Speicmen
- 4 - Speicmen stands
- 5 - Strain gage
- 6 - Mid-span

Figure 8. Test facility

the stress-strain curve of tensile UHPC before the appearance of visible cracks, strain gages were placed at the bottom, 5 mm from the bottom at one flank, and the initial neutral axis of the specimens as shown in Figure 8a. To ensure the accuracy of the test results, the loading control is based on mid-span displacement with a slow loading rate of 0.5 mm per minute and the strain data-collection frequency is 10 Hz.

Table 2. UHPC Ingredients, kg/m<sup>3</sup>

Cement	Silica sand	Silica fume	Modified additive	Steel fibre	Water
875	900	250	25	200	190

### 3.2.2. Test results

Three specimens were tested. The typical load-midspan displacement is shown in Figure 9.

The results show that four stages were observed from the load-displacement curve. Stage I is steady and quasi-linear stage without visible cracking. The load-displacement curve moves into Stage II with the appearance of visible cracks and the first inflection point. The calculated cracking bending moment is 2.6 kNm. During Stage II, tiny visible cracks keep forming in the tensile region of the specimen. The development of these visible cracks is slow due to the reinforcing effect arising from fibre bridging. The bridging force is sufficient to limit the expansion of these visible cracks; therefore, the bearing capacity at Stage II is able to increase unsteadily and non-linearly. After the second inflection point, the load-displacement curve moves into Stage III, which is the yield stage. The carrying capacity at Stage III fluctuates within a small range and the displacement continues to increase. The calculated bending moment is 37.5 kNm, and the displacement limit is 0.88 mm. The yield stage indicates the generation of the main crack and the bridging

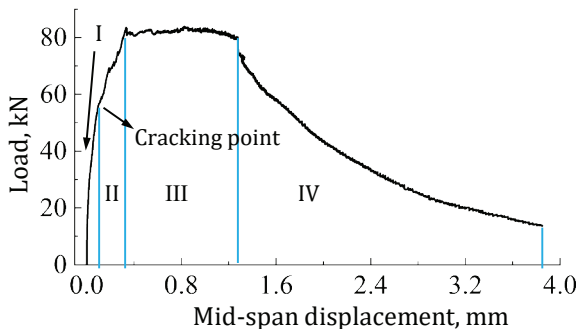


Figure 9. LVDT Displacement under bending condition

effect cannot further limit the expansion of the crack. Therefore, upon the development of the main crack, more fibres contribute to the aforementioned bridging. Stage III is a dynamic balance stage. After the bridging effect reaches its limit, the curve enters Stage IV, which is the failure stage. Most of the fibre is pulled out from cement matrix with the propagation of the main crack.

For the first Stage I, the stress mechanism of steel fibre is investigated by the micro-analysis method. To verify the two stages before the onset of visible cracking, the Stage I displacement-strain curve of the initial neutral axis is shown in Figure 10a. When the load reaches 12 kN and the mid-span displacement is 0.03–0.04 mm, the strain of the initial neutral axis begins to increase. Each set of the specimens indicates that the actual neutral axis is moving with the development of the mid-span displacement. The movement of the neutral axis demonstrates convincingly that there are two different stages within Stage I, which is the steady quasi-linear stage without any

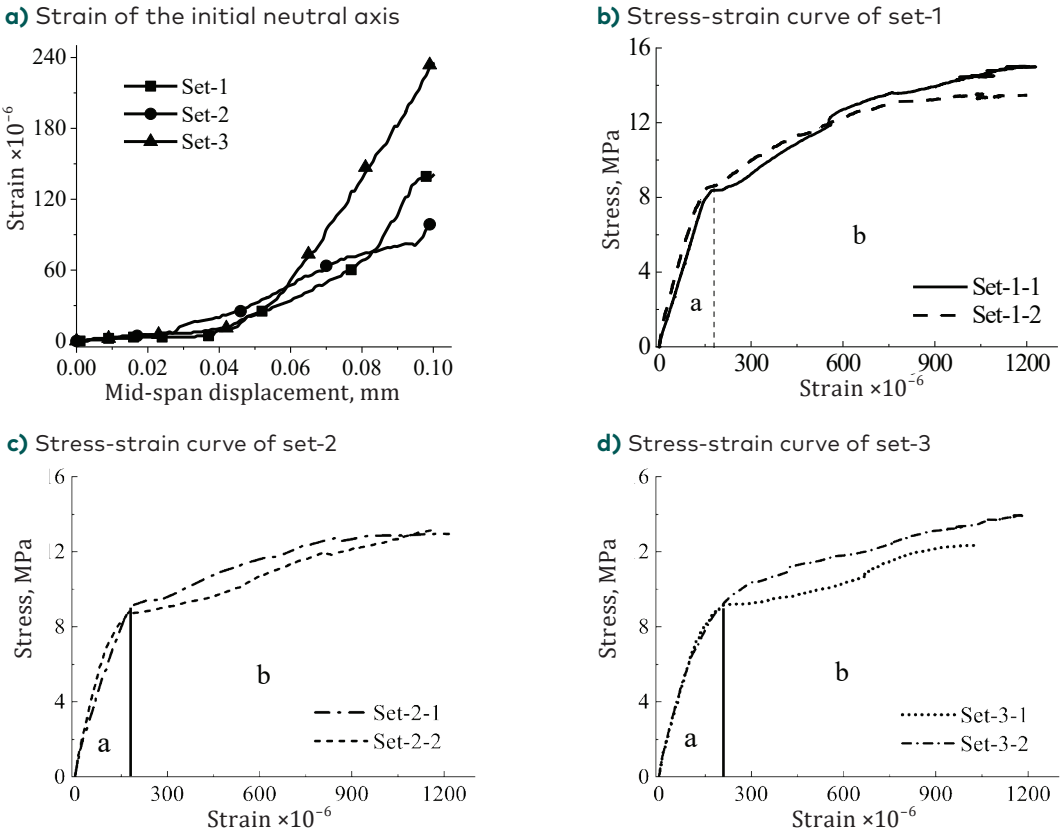


Figure 10. Four-point bending test data

visible cracks. The stress-strain curves of each specimen are shown in Figures 10b to 10d.

There are two stages with different slopes and stabilities before the appearance of visible cracks (Stage a and Stage b as shown in Figure 10). Compared with the predictive model, Stage a is the elastic stage and Stage b is micro-damage development stage. Six sets of data have a similar growth trend in the elastic stage, which is smooth and stable. The average elastic limit is 8.9 MPa and 180  $\mu\epsilon$ , because such cracks can directly damage the strain gages. The limitation of the micro-damage development stage is defined by the singularity of strain data. The data of the micro-damage development stage show irregular growth while the average cracking values are 13.49 MPa and 1176  $\mu\epsilon$ .

### 3.2.3. Verification of the micro-analysis method

The micro-analysis method can be used to describe the test phenomenon of the two-stage stress-strain curve. Based on the micro-analysis method, the bonding mechanism of steel fibre loaded by

Table 3. Test and theoretical limitation of elastic limit

Specimen set	Tests stress, MPa	Test strain ( $\times 10^{-6}$ )	Elasticity Modulus, GPa	Theoretical values	Percentage of stress difference, %
Set-1-1	8.76	167	52.45	Stress, MPa	1.02
Set-1-2	8.56	173	49.48	8.85	3.38
Set-2-1	8.72	170	51.29	Strain ( $\times 10^{-6}$ )	1.49
Set-2-2	9.25	194	47.68	180	4.32
Set-3-1	9.12	192	47.50	Elasticity Modulus, GPa	2.96
Set-3-2	9.02	186	48.50	49.17	1.88

Table 4. Test limitation of the micro-damage development stage

Specimen set	Test stress, MPa	Test strain $\times 10^{-6}$
Set-1-1	15.02	1178
Set-1-2	13.47	1196
Set-2-1	12.95	1215
Set-2-2	13.19	1175
Set-3-1	12.36	1022
Set-3-2	13.96	1270
CV	6.80%	7.06%

cement matrix is different under axial tension and bending. Due to the linear distribution of bending strain, the elastic modulus under bending is slightly lower than the axial tension. The tests of UHPC material performance show that the elastic modulus is 50 GPa under axial tension. The test and theoretical values are summarised in Table 3. The results indicate that the calculated stress match the test data. The micro-analysis method of the elastic stage is thus deemed both reasonable and accurate.

Differing from the elastic assumption adopted before visible cracking (Zhang et al., 2015), the micro-analysis method defines the micro-damage development stage, which is stochastic and in dynamic equilibrium. The stress-strain curves are difficult to unify and the limitations are listed in Table 4.

The development of the micro-damage is random and unpredictable. None of these data can be fitted by a single elementary function and the ultimate stress and strain varies: the coefficient of variation of strain is smaller than that of stress at 6.80% and 7.06%, respectively. The phenomenon of the micro-damage development stage can be explained by the micro-analysis method. The clear understanding of the fibre tensile behaviour contributes to guiding the design process. Therefore, the micro-analysis method is necessary.

With the increasing of the tensile deformation, the essential difference between the elastic stage and the micro-damage development stage is the loss of steel fibre reinforcement. The micro-analysis method can be simplified for engineering application and two limiting values for each stage are chosen for the bilinear model based on the test results. The limit strain of the elastic stage can take the average values, which

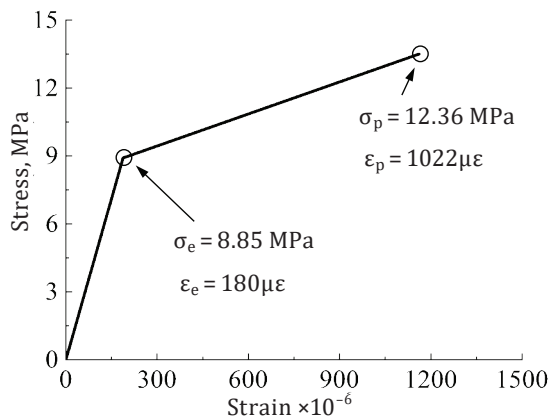


Figure 11. Simplified constitutive bilinear model

are 8.9 MPa and 180  $\mu\epsilon$ . The limit to the micro-damage development stage should take the minimum value 1022  $\mu\epsilon$  to avoid visible cracking shown in Figure 11.

Thus, the bilinear constitutive model under bending condition for the UHPC specimens tested can be given by:

$$\sigma(\epsilon) = \begin{cases} E_1\epsilon, & 0 < \epsilon \leq \epsilon_e \\ E_2\epsilon, & \epsilon_e < \epsilon \leq \epsilon_p \end{cases}$$
$$\sigma_e = E_1\epsilon_e,$$
$$\sigma_p = E_2\epsilon_p,$$

where the  $\sigma_e$  and  $\epsilon_e$  are limit stress and strain at the elastic stage, and  $\sigma_p$  and  $\epsilon_p$  are the ultimate stress and strain at the micro-damage development stage. The proposed bilinear constitutive model shown in Figure 11 uses two line-segments to describe the stress-strain relationship of tensile UHPC. The elastic modulus in the first stage is 49.17 GPa, and in the second stage it is 4.17 GPa.

## Conclusions

The main conclusions are summarised as follows:

1. The method calculation treating UHPC as a composite structure is reasonable. The tensile properties of UHPC are dominated by the internal steel fibre. The contribution of the cement matrix to the axial force on the UHPC under tensile load can be ignored.
2. The micro-analysis method can describe the non-uniform stress distribution on steel fibre which is consistent with the reactive force properties thereof. Theoretical results indicate that there are two different stress patterns measured in the steel fibre before the appearance of visible cracking: the first is the elastic stage and the second is in the micro-damage development stage.
3. The predicted elastic stage and micro-damage development stage are verified by test and published data. The difference between the elastic stage and the micro-damage development stage is analysed as the shift of fibre stress patterns caused by micro-damage, indicating the weakening of the fibre reinforcement as affected by the loss of effective working length.
4. The stress-strain curves predicted by micro-analysis method can be simplified to a bilinear model for engineering application. For the tested UHPC, the limiting values of the smooth and stable elastic stage are 8.85 MPa and 180  $\mu\epsilon$ . Due to test data scatter, the minimum

strain  $1022 \mu\epsilon$  is used to denote the limit of the micro-damage development stage required to avoid cracking.

## Funding

The study has been funded by the National Natural Science Foundation of China under Grant [numbers 52268027].

## REFERENCES

- Aaleti, S., Petersem, B., & Sritharan, S. (2013). *Design guide for precast UHPC waffle deck panel system, including connections* (Report No. FHWA-HIF-13-032). Washington DC: Federal Highway Administration. <https://www.fhwa.dot.gov/hfl/partnerships/uhpc/hif13032/hif13032.pdf>
- AFGC/SETRA. (2013). *Ultra-high performance fibre reinforced concrete*. Paris: Association française de normalisation.
- Ai-Osta, M. A., Isa, M. N., Baluch, M. H., & Rahman, M. K. (2017). Flexural behaviour of reinforced concrete beams strengthened with ultra-high performance fibre reinforced concrete. *Construction and Building Materials*, 134, 279–296. <https://doi.org/10.1016/j.conbuildmat.2016.12.094>
- Barros, J. A., Cunha, V. M., Ribeiro, A. F., & Antunes, J. A. B. (2005). Post-cracking behaviour of steel fibre reinforced concrete. *Materials and Structures*, 38(1), 47–56. <https://doi.org/10.1007/BF02480574>
- Chan, Y. W., & Chu, S. H. (2004). Effect of silica fume on steel fibre bond characteristics in reactive powder concrete. *Cement and Concrete Research*, 34(7), 1167–1172. <https://doi.org/10.1016/j.cemconres.2003.12.023>
- Dogu, M., & Menkulasi, F. (2020). A flexural design methodology for UHPC beams posttensioned with unbonded tendons. *Engineering Structures*, 207, Article 110193. <https://doi.org/10.1016/j.engstruct.2020.110193>
- Ghafari, E., Costa, H., Julio, E., Portugal, A., & Duraes, L. (2014). The effect of nanosilica addition on flowability, strength and transport properties of ultra high performance concrete. *Materials & Design*, 59, 1–9. <https://doi.org/10.1016/j.matdes.2014.02.051>
- Graybeal, B. A. (2006). *Material property characterization of ultra-high performance concrete* (Report No. FHWA-HRT-06-103). Federal Highway Administration. <https://www.fhwa.dot.gov/publications/research/infrastructure/structures/06103/06103.pdf>
- Guo, Z. H. (1997). *Strength and deformation of concrete: Test and constitutive relation*. Beijing: Tsinghua University Press (in Chinese).
- Habel, K., Denare, E., & Brühwiler, E. (2004). Structural response of composite “UHPFRC-Concrete” members under bending. *International Symposium on Ultra High Performance Concrete (UHPC'04)*, 389–399.
- Huang, C. K. (2004). *Fibre reinforced concrete structure*. Beijing: China Machine Press (in Chinese).

- Johnston, C. D. (2001). *Fibre reinforced cements and concretes*. Amsterdam, Netherlands: Gordon and Breach Science Publishers.
- Kang, S. H., Ji-Hyung, L., Hong, S. G., & Moon, J. (2017). Microstructural investigation of heat-treated ultra-high performance concrete for optimum production. *Materials*, 10(9), Article 1106. <https://doi.org/10.3390/ma10091106>
- Kang, S., & Kim, J. (2011). The relation between fibre orientation and tensile behaviour in an ultra high performance fibre reinforced cementitious composites (UHPFRCC). *Cement and Concrete Research*, 41(10), 1001–1014. <https://doi.org/10.1016/j.cemconres.2011.05.009>
- Lee, M. K., & Barr, B. I. G. (2004). An overview of the fatigue behaviour of plain and fibre reinforced concrete. *Cement and Concrete Composites*, 26(4), 299–305. [https://doi.org/10.1016/S0958-9465\(02\)00139-7](https://doi.org/10.1016/S0958-9465(02)00139-7)
- Liang, X. W., & Shi, Q. X. (2011). *Design principle of concrete structure*. Beijing: China Architecture and Building Press. (in Chinese)
- Lok, T. S., & Pei, J. S. (1998). Flexural behaviour of steel fibre reinforced concrete. *Journal of Materials in Civil Engineering*, 10(2), 86–97. [https://doi.org/10.1061/\(ASCE\)0899-1561\(1998\)10:2\(86\)](https://doi.org/10.1061/(ASCE)0899-1561(1998)10:2(86))
- Noori, A., Shekarchi, M., & Moradian, M. (2015). Behaviour of steel fibre-reinforced cementitious mortar and high-performance concrete in triaxial loading. *ACI Materials Journal*, 112(1), 95–104. <https://doi.org/10.14359/51686837>
- Orange, G., Acker, P., & Vernet, C. (1999). A new generation of UHP concrete: Ductal, damage resistance and micromechanical analysis. *Third International Workshop on High Performance Fibre Reinforced Cement Composites (HPFRCC3)*, Mainz, Germany, 101–111.
- Park, S. H., Dong, J. K., Ryu, G. S., & Koh, K. T. (2012). Tensile behaviour of ultra high performance hybrid fibre reinforced concrete[J]. *Cement and Concrete Composites*, 34(2), 172–184. <https://doi.org/10.1016/j.cemconcomp.2011.09.009>
- Qi, J., Wang, J., & Ma, Z. (2018). Flexural response of high-strength steel-ultra-high-performance fibre reinforced concrete beams based on a mesoscale constitutive model: Experiment and theory. *Structural Concrete*, 19(3), 719–734. <https://doi.org/10.1002/suco.201700043>
- Randl, N., Steiner, T., Ofner, S., Baumgartner, E., & Meszoly, T. (2014). Development of UHPC mixtures from an ecological point of view. *Construction and Building Materials*, 67(C), 373–378. <https://doi.org/10.1016/j.conbuildmat.2013.12.102>
- Rilem, T. C. (2003). Test and design methods for steel fibre reinforced concrete,  $\sigma$ - $\omega$  design method. *Materials and Structures*, 36, 560–567. <https://www.rilem.net/images/publis/1507.pdf>
- Russell, H. G., & Graybeal, B. A. (2013). *Ultra-high performance concrete: A state-of-the-art report for the bridge community* (Report No. FHWA-HRT-13-060). Federal Highway Administration. <https://www.fhwa.dot.gov/publications/research/infrastructure/structures/hpc/13060/13060.pdf>

- Shao, X. D., LI, F. Y., Qiu, M. H., et al. (2020). Influential and comparative research on the effects of steel fibre properties on the axial tensile and bending tensile properties of UHPC. *China Journal of Highway and Transport*, 33(4), 51–64. (in Chinese)
- Shen, D. Y. (2017). *The basic research on the flexural properties of ultra high performance concrete* [M.A. Thesis]. Changsha: Hunan University. (in Chinese)
- Singh, H. (2015). Flexural modeling of steel fibre-reinforced concrete members: Analytical investigations. *Practice Periodical on Structural Design and Construction*, 20(4), 1–10.  
[https://doi.org/10.1061/\(ASCE\)SC.1943-5576.0000244](https://doi.org/10.1061/(ASCE)SC.1943-5576.0000244)
- Van, Z. G., & Mbewe, P. (2013). Flexural modelling of steel fibre-reinforced concrete beams with and without steel bars. *Engineering Structures*, 53, 52–62. <https://doi.org/10.1016/j.engstruct.2013.03.036>
- Wille, K., & Naaman, A. E. (2012). Pullout behaviour of high-strength steel fibres embedded in ultra-high-performance concrete. *ACI Materials Journal*, 109(4), 479–487. <https://doi.org/10.14359/51683923>
- Wille, K., & Naaman, A. E. (2010). Bond stress-slip behaviour of steel fibres embedded in ultra high performance concrete. *Proceedings of 18th European Conference on Fracture and Damage of Advanced Fibre-Reinforced Cement matrixed Materials*, 99–111. <https://www.gruppofrattura.it/ocs/index.php/esis/ECF18/paper/viewFile/6376/2237>
- Zhang, Z., Shao, X. D., & Li, W. G. (2015). Axial tensile behaviour test of ultra high performance concrete. *China Journal of Highway and Transport*, 28(8), 50–58. (in Chinese)
- Zhang, Z. (2016). Bending behaviours of composite bridge deck system composed of OSD and reinforced UHPC layer [Ph.D. Thesis, Changsha: Hunan University]. (in Chinese)